Output-Only Vibration-Based Monitoring of Civil Infrastructure via Sub-Nyquist/Compressive Measurements Supporting Reduced Wireless Data Transmission

Kyriaki Gkoktsi[1], Agathoklis Giaralis[1]*, Roman P. Klis[2], Vasilis Dertimanis[2] and Eleni N. Chatzi[2]

[1] Department of Civil Engineering, City, University of London, London, United Kingdom, [2] Department of Civil, Environmental and Geomatic Engineering, ETH Zürich, Zurich, Switzerland

The consideration of wireless acceleration sensors is highly promising for cost-effective output-only system identification in the context of operational modal analysis (OMA) of large-scale civil structures as they alleviate the need for wiring. However, practical monitoring implementations for OMA using wireless units suffer a number of drawbacks related to wireless transmission of densely sampled acceleration time-series including the energy self-sustainability of the sensing nodes. In this work, two recently proposed approaches for output-only modal identification addressing the above issues through balancing monitoring accuracy with data transmission costs are comparatively studied and numerically assessed using field recorded acceleration datasets from two different structures: (i) an operating on-shore wind turbine, (ii) an open to traffic highway bridge. One approach utilizes non-uniform-in-time deterministic multi-coset sampling at sub-Nyquist rates to capture structural response acceleration time-series under ambient excitation assuming stationary signal conditions. In this approach, a power spectrum blind sampling technique is used to estimate the response acceleration power spectral density matrix from the low-rate sampled measurements and is coupled with the Frequency Domain Decomposition method of OMA. The other is a spectro-temporal compressive sensing approach which recovers response acceleration signals through time-series reconstruction in the time domain from sub-Nyquist non-uniform-in-time randomly sampled measurements. Prior knowledge of signal structure in the spectral domain is exploited through smart on-sensor operations and sensor/server communication. The benefits and limitations of the considered approaches are discussed and demonstrated by processing the field recorded datasets for different levels of signal compression and by estimating battery lifetime gains at a single sensor achieved by reduced data transmission. It is concluded that the two approaches are readily applicable in OMA of large-scale structures and can be used complementarily depending on the requirements of any particular acceleration monitoring campaign: time-series extraction for further interrogation vs. solely modal properties estimation.

Keywords: vibration-based modal identification, multi-coset sampling, spectro-temporal compressive sensing, blind power spectrum sampling, operational modal analysis, wireless sensors

INTRODUCTION

In recent years, monitoring schemes have roved their worth in terms of the potential for smart operation and maintenance of civil structures (Farrar and Worden, 2012). When further coupled with the concept of the Value of Information, monitoring of structures serves as a direct tool for informing decision support on the life cycle management of structural assets. In this context, operational modal analysis (OMA) involves an efficient monitoring modality in large scale structural systems, as it is typically enabled by low cost acceleration sensors, allowing for a long-term or permanent system supervision (Limongelli et al., 2016). Due to the difficulty involved in the measurement of operating loads, OMA relies on output-only information for extraction of dynamic properties of systems that are typically subjected to low-amplitude operational loads (e.g., due to wind traffic, etc.) (Brincker and Ventura, 2015). For the common case of linear systems, such properties include the modal characteristics of the structure (e.g., natural frequencies, damping and mode shapes). Since no explicit loading information is assumed available, output-only techniques commonly assume ambient conditions corresponding to a flat spectrum over a wide range of frequencies (i.e., a white noise excitation assumption). Such techniques are shown to perform well, even under the challenge of varying environmental and operational conditions (Reynders et al., 2013; Shi et al., 2016; Avendaño-Valencia et al., 2017) while the extracted modal structural properties may be then exploited for a variety of tasks including condition assessment, design verification, structural health monitoring (SHM) and, ultimately, residual life prediction of civil structures (Straub et al., 2017). Still, OMA has been mostly demonstrated for use with tethered sensing configurations.

Wireless sensor networks (WSNs) offer a low-cost and easily deployable alternative to tethered (wired) acceleration sensors that is particularly attractive for large structures featuring locations of reduced accessibility (Lynch, 2007). The "smart" feature of most such wireless platforms, allowing for local processing at the wireless senor (node) level, has been exploited for decentralized autonomous monitoring solutions (Nagayama et al., 2009). Nonetheless, WSNs have so far not enjoyed widespread adoption into practice, largely owing to their limited wireless transmission bandwidth and the maintenance costs related to frequent battery replacement (Klis and Chatzi, 2016a; Gkoktsi and Giaralis, 2019).

In order to extend the self-sustainability of the nodes, and to reduce the power allocated for transmission, compressive sensing (CS) techniques have been explored, with Bao et al. (2010) and O'Connor et al. (2013), leading developments in this field, with applications on actual road bridges. CS samples at random non-uniform in time rates, resulting in equivalent sampling below the Nyquist rate. In a nutshell, CS asserts that a discrete-time finite length signal (e.g., an analog response acceleration signal uniformly sampled in time) can be recovered, with high probability, from a relatively small number of randomly acquired samples/measurements in time, by solving an underdetermined system of linear equations (Candès and Tao, 2006; Donoho, 2006). Importantly, the number of random (compressed) measurements required for a faithful signal recovery depends on the "sparsity" of the acquired signal with respect to some pre-specified vector basis, such as the discrete Fourier transform (DFT) basis used for representation of vectors in the Fourier/frequency domain. Specifically, a K-sparse/compressible signal features K expansion coefficients on a given basis with values larger than a relatively low threshold; the smaller K is, the sparser the signal is, and thus the fewer random measurements are required for its sparse recovery (i.e., estimation of the K significant expansion coefficients) within the CS framework. In this regard, all algorithms for sparse signal recovery necessitate an assumption of signal sparsity (Vaswani and Zhan, 2016), which is *a priori* unknown and is adversely affected by signal noise. Further, much research work has been devoted in constructing sparsifying bases or, more generally, sparsifying dictionaries tailored for different applications, such as image denoising (Razaviyayn et al., 2014), video sensing (Eslani et al., 2014), and ultrasonic non-destructive damage detection (Fuentes et al., 2019).

In this setting, O'Connor et al. (2014) were the first to deploy customized CS-based wireless sensors in a long-term monitoring field application for an overpass in MI, USA. By randomly triggering in time conventional ADC units, non-uniform in time compressed acceleration response signals were acquired. Sparse recovery assuming a DFT expansion basis, as well as an empirically specified level of sparsity was applied to the compressed data to estimate the response acceleration power spectral density (PSD) matrix. The latter matrix was used in conjunction with the standard frequency domain decomposition (FDD) algorithm to extract mode shapes and natural frequencies within OMA. Yang and Nagarajaiah (2015) and Park et al. (2014) contributed two significantly different approaches for mode shape estimation from CS-based non-uniform in time random sampling of structural vibration time-histories at sub-Nyquist rates. In Yang and Nagarajaiah (2015) mode shape estimation relies on modal structural responses obtained by application of blind source separation directly to the compressed measurements of structural response signals. Sparse signal recovery (reconstruction) in the time-domain is next applied to each compressed modal response vector to retrieve the underlying structural natural frequencies and modal damping ratios. In Park et al. (2014) mode shapes are obtained by means of a singular value decomposition-based algorithm applied directly to response acceleration compressed measurements, without taking any reconstruction step, under the assumption of noiseless undamped free vibration structural response signals (i.e., multi-tone signal model).

The standard approach to CS-based signal recovery relies on l_1-norm minimization and solution of the so-called Basis Pursuit De-Noising problem (BPDN). This approach is typically adopted in CS implementations in OMA applications using wireless sensors (O'Connor et al., 2014; Zou et al., 2015). In enhancing the BPDN approach, Klis and Chatzi (2016b) utilize its re-weighted variant, known as the re-weighted Basis Pursuit De-Noising problem (rwBPDN), also known as the l_1-analysis problem (Becker et al., 2011). The resulting Spectro-temporal CS (STCS) scheme leads to improved time-domain signal recovery

with respect to the standard BPDN approach. Furthermore, in order to alleviate the heuristic *a priori* assumption on sparsity Klis and Chatzi (2016a) initially exploit the concept of a leading node, i.e., a (typically) tethered node which is permanently logging at higher sampling rates, and forms part of a Hybrid Sensor Network (HSN). The latter forms a compilation of primarily wireless and a minimal number of tethered sensors. In this way the signal support, on the basis of which the recovery is performed, is narrowed, which results in reduced transmission costs. In later work (Klis and Chatzi, 2016b) the leading node requirement is removed, with wireless sensors transmitting partial temporal information and a selected part of the spectral information in a two way communication with the server (central node). Sparse signal recovery is again enabled via solution of the rwBPDN problem. The recovered signals may then serve as input for any standard output-only modal identification algorithm for OMA. As signal reconstruction is a main target of this approach, it is particularly attractive for use with time domain-based identification methods, such as approaches based on Auto-regressive models, subspace identification algorithms, or real-time tracking using Kalman filters. The proposed scheme has been validated on synthetic simulations generated for a benchmark four-story frame structure of the American Society of Civil Engineers, as well as data from operating structures.

Aiming to circumvent the signal sparsity requirement for the identification of modal characteristics (natural frequencies and modal shapes) from sub-Nyquist sampled response acceleration data, Gkoktsi and Giaralis (2017), Gkoktsi and Giaralis (2019) developed an alternative to the former CS-based approaches. The latter approach couples the sub-Nyquist non-uniform-in-time deterministic multi-coset sampling strategy (Venkataramani and Bresler, 2001), with a Power Spectrum Blind Sampling (PSBS) technique (Ariananda and Leus, 2012; Tausiesakul and González-Prelcic, 2013) extended to the multi-channel case by Gkoktsi et al. (2015) to estimate the response acceleration PSD matrix (second order statistics) from correlation sequences of the sub-Nyquist measurements. Ultimately, the considered PSBS approach derives structural modal properties by application of the FDD algorithm to the estimated PSD matrix without response acceleration signal recovery in the time domain and without making an *a priori* assumption on signal sparsity in the DFT or in any other domain (Gkoktsi and Giaralis, 2017). In doing so, measured response signals are assumed as stationary correlated stochastic processes in alignment with OMA theory (Brincker and Ventura, 2015). In this respect, the PSBS approach does not return the time-histories of acceleration response signals but, on the positive side, it is purely signal agnostic in terms of signal structure in the frequency domain and, therefore, indifferent to signal sparsity attributes and/or to additive noise. In this regard, it was shown that the PSBS approach achieves quality mode shape extraction and robust modal strain-based damage detection from response acceleration measurements corrupted by additive noise (Gkoktsi et al., 2016) at rates as low as 80% below Nyquist leading to significant energy consumption gains in wireless sensors (Gkoktsi and Giaralis, 2019).

Previously, the PSBS approach has been compared to standard BPDN CS-based approach in terms of quality mode

shape extraction (Gkoktsi and Giaralis, 2017). Herein, we comparatively assess the PSBS-based scheme (Gkoktsi and Giaralis, 2017, 2019) and the STCS approach (Klis and Chatzi, 2016a,b) in an effort to demonstrate their readiness levels for output-only modal identification supported by low-power wireless sensors which is the first step toward cost-effective SHM. The strengths and limitations of each approach are elaborated upon, with a comparison in terms of data compression, potential for modal identification, and, for the case of STCS, on time-domain signal recovery. In order to validate the presented tools, field data from large scale structures are utilized, namely acceleration response time-histories from an operating on-shore wind turbine as well as from a highway overpass open to traffic. For the second structure, estimated battery lifetime gains at the sensor node level are provided achieved by power consumption savings from reduced wireless data transmission.

METHODOLOGICAL FRAMEWORK

Spectro-Temporal Compressive Sensing (STCS) Approach via *rwBPDN*

Spectro-Temporal Compressive Sensing (*STCS*) relies on the formulation of the *missing data estimation problem* (Candès and Romberg, 2007; Becker et al., 2011; Candès and Plan, 2011). Let us assume a signal recorded by sensor i, comprising N samples. The *missing data estimation problem* is formulated as:

$$\mathbf{y}_i = \mathbf{S}\mathbf{x}_i \tag{1}$$

where $\mathbf{y}_i = [y_{1i}, y_{2i}, ..., y_{Mi}]^T \in \mathbb{R}^M$ is the measured signal of partial (incomplete) observations, comprising a dimension $M < N$, and $\mathbf{S} \in \mathbb{R}^{M \times N}$ is a zero-one selection matrix, known a-priori. The goal of the missing data estimation problem is to recover the original full signal $\mathbf{x}_i$ given the incomplete observations $\mathbf{y}_i$ and the selection matrix $\mathbf{S}$.

As demonstrated in Klis and Chatzi (2016b) structural response signals admit a sparse representation via a Discrete Fourier Transform (DFT) orthonormal basis, $\mathbf{A} \in \mathbb{C}^{N \times N}$, according to the following equation:

$$\mathbf{x}_i = \mathbf{A}\mathbf{c}_i, \text{ where } \mathbf{A}_{i,l} = \frac{1}{\sqrt{N}} e^{-j2\pi i \frac{l}{N}} \tag{2}$$

where $\mathbf{c}_i = [c_{1i}, c_{2i}, ..., c_{Ni}]^T \in \mathbb{R}^N$ comprises the coefficient vector. Via substitution of equation (2) into equation the observations vector $\mathbf{y}_i$ may be recovered on the basis of a finite number of $\mathbf{c}_i$ sparse coefficients, as follows:

$$\mathbf{y}_i = \mathbf{S}\mathbf{A}\mathbf{c}_i \tag{3}$$

When the vector of observations $\mathbf{y}_i$ is incomplete, as is the case for missing data, equation (3) comprises an ill-conditioned problem with multiple solutions for the coefficients vector $\mathbf{c}_i$. Within the compressive sensing context however, we are interested in the solution rendering the most sparse vector $\mathbf{c}_i$, for which equation (1) is fulfilled. This is recovered via

solution of a non-deterministic polynomial time-Hard (NP-Hard) combinatorial problem:

$$\arg\min_{\mathbf{c}_i} \|\mathbf{c}_i\|_0 \quad \text{subject to} \quad \mathbf{y}_i = \mathbf{SAc}_i \tag{4}$$

As the formulation of equation (4) is non-trivial to solve, Candès and Romberg (2007) concluded that solving a relaxed $\|\cdot\|_1$ convex optimization problem, known as a *basis pursuit problem*, is equivalent to solving the original $\|\cdot\|_0$ NP-Hard combinatorial problem, given that an appropriate condition—the so-called *Restricted Isometry Property (RIP)*—holds. The *basis pursuit problem* is expressed as:

$$\arg\min_{\mathbf{c}_i} \|\mathbf{c}_i\|_1 \quad \text{subject to} \quad \mathbf{y}_i = \mathbf{SAc}_i \tag{5}$$

The formulation of equation offers a significant reduction in terms of computational toll, while guaranteeing that the original response signal $\mathbf{x}_i$ may be fully recovered, provided that the K-RIP condition is satisfied by matrix $\mathbf{SA}$. For each positive integer K, we may define the isometry constant δ_K of matrix $\mathbf{SA}$ as the smallest integer ensuring that the following K-RIP condition holds for all K-sparse vectors:

$$(1 - \delta_K)\|\mathbf{c}_i\|_2^2 \leq \|\mathbf{SAc}_i\|_2^2 \leq (1 + \delta_K)\|\mathbf{c}_i\|_2^2 \tag{6}$$

According to Candès et al. (2006) if $\delta_{2K} < \sqrt{2} - 1$ then a solution to (5) will also satisfy the original problem (4) with a good quality of approximation.

However, observations stemming from acquisition via sensor nodes, as is typical for SHM measurements, will be corrupted with noise. In this case, the original problem becomes

$$\mathbf{y}_i = \mathbf{SAc}_i + \mathbf{z}_i, \ \mathbf{z}_i \propto \mathcal{N}(0, \sigma^2) \tag{7}$$

The solution to this modified problem is obtained via a convex optimization problem, known as the *Basis Pursuit De-Noising problem* (BPDN):

$$\arg\min_{\mathbf{c}_i} \|\mathbf{c}\|_1 \quad \text{subject to} \quad \|\mathbf{y}_i - \mathbf{SAc}_i\|_2 \leq \epsilon \tag{8}$$

Solution of the BPDN problem has been the main approach utilized so far in the context of CS for SHM implementations (O'Connor et al., 2014; Wang and Hong, 2015; Wang et al., 2015). Klis and Chatzi (2016b) have advanced this framework by utilizing in lace of the classical BPDN formulation, its re-weighted variant, known as the *re-weighted Basis Pursuit De-Noising problem (rwBPDN)* (Becker et al., 2011):

$$\arg\min_{\mathbf{c}_i} \|\mathbf{Wc}_i\|_1 \quad \text{subject to} \quad \|\mathbf{y}_i - \mathbf{SAc}_i\|_2 \leq \epsilon \tag{9}$$

Key to this formulation is the weighting matrix $\mathbf{W} = diag([w_1, w_2, ..., w_N])$ which ensures a desired structure of the coefficient vector $\mathbf{c}_i$.

The Spectro-Temporal Compressive Sensing (STCS) framework relies on solution of the *rw-BPDN* problem. **Figure 1** illustrates the steps of STCS framework, with the actions performs locally on the node level aggregated on the left, and actions performed globally at the base station (server) level assembled on the right. As a first step, the support is determined at each node. The support of a vector is defined as the subset of non-zero components $supp(\mathbf{Y}_i) = \{\omega \in \mathbf{\Omega} : \mathbf{Y}_i(\omega) \neq 0\}$. For practical implementations, this is eventually defined in terms of exceedance of a user-specified threshold ϵ : $supp(\mathbf{Y}_i, \epsilon) = \{\omega \in \mathbf{\Omega} : |\mathbf{Y}_i(\omega)| > \epsilon\}$. The selection of the support is executed for windowed frames $\mathbf{x}_{ij}$, extracted from the original signal $\mathbf{x}_i$. The formulated support $\mathbf{U}_{ij}$, as well as its complementary set $\mathbf{U}_{ij}^c$ allow the decomposition of the spectral representation of the signal, as expressed via the coefficient vector $\mathbf{c}_i$, into a "noisy" and "clean" component $\mathbf{c}_{ij} = \mathbf{U}_{ij}\mathbf{c}_{ij} + \mathbf{U}_{ij}^c\mathbf{c}_{ij}$. The locally defined support components are eventually transmitted to the server, where the weighting matrix $\mathbf{W}_{ij}$ is formulated and the K-sparsity of the signal is determined as $K_{ij} = \sum(\mathbf{U}_{ij})$.

In a next step, the number of time-domain samples M_{ij} required for signal recovery is defined, on the basis of which the server randomly selects and transmits $\mathbf{y}_{ij}$ sub-vectors, from the j-th data frame of the i-th sensor, using a uniform distribution. For more details on this process the interested reader is referred to (Klis and Chatzi, 2016b). Upon transmission of the necessary time domain samples, along with the corresponding $\mathbf{W}_{ij}$ weighting matrix, to the server the coefficient vector is recovered as $\hat{\mathbf{c}}_{ij} = \arg\min_{\mathbf{c}_{ij}} \|\mathbf{W}_{ij}\mathbf{c}_{ij}\|_1$ subject to $\|\mathbf{y}_{ij} - \mathbf{S}_{ij}\ma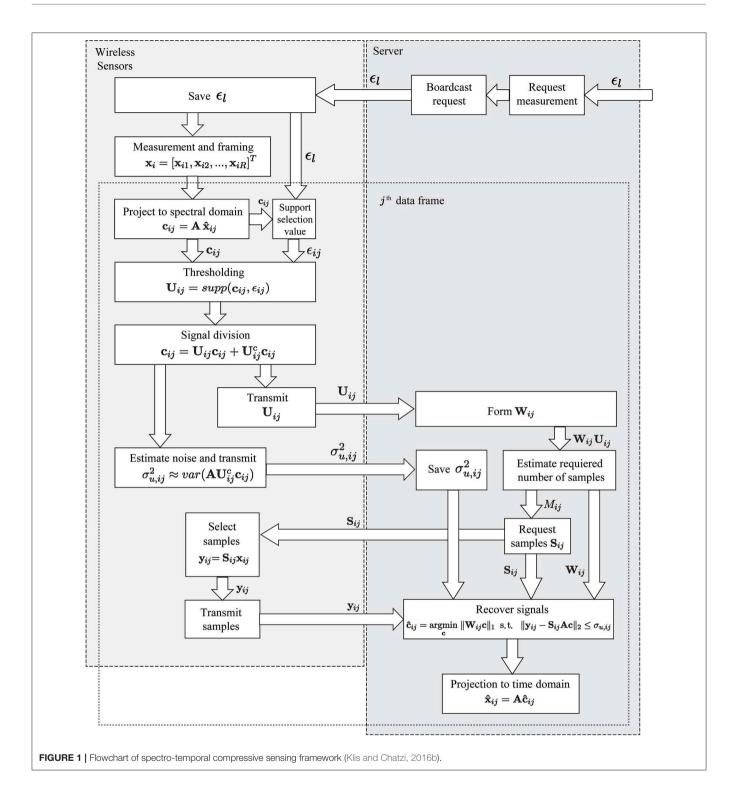thbf{Ac}_{ij}\|_2 \leq \sigma_{u,ij}$. As a last step, the coefficient vector of the j-th data frame is projected back to the time domain:

$$\hat{\mathbf{x}}_{ij} = \mathbf{A}\hat{\mathbf{c}}_{ij} \tag{10}$$

Once this process has been executed for each data frame, the estimate of the full time domain signal is attained as $\hat{\mathbf{x}}_i = \left[\hat{\mathbf{x}}_{i1}, \hat{\mathbf{x}}_{i2}, ..., \hat{\mathbf{x}}_{iD}\right]^T$ from all D sensors in the network. The solver adopted for solution of the involved *rwBPDN* problem is the NESTA algorithm (Nesterov, 2005; Becker et al., 2011).

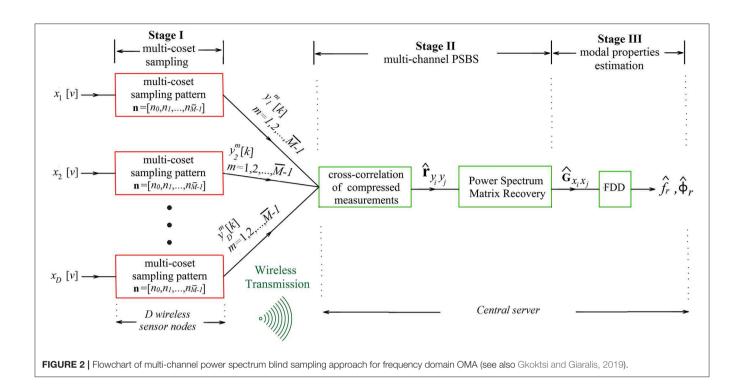## The Multi-Channel Power Spectrum Blind Sampling (PSBS) Approach

The multi-channel PSBS approach for operational modal analysis developed by Gkoktsi and Giaralis (2017), Gkoktsi and Giaralis (2019) comprises the three stages delineated in **Figure 2**. The first stage involves low-rate (sub-Nyquist) deterministic periodic non-uniform-in-time multi-coset sampling at all D acceleration sensing nodes. In the next stage, the low-rate (compressed) measurements from all sensors are wirelessly transmitted to a server (base station) and centrally processed to obtain their cross-correlation vectors. These vectors are used to estimate (recover) the response acceleration PSD matrix by solving an overdetermined system of linear equations without invoking any signal sparsity assumption. Lastly, in stage III, the FDD algorithm is applied to the recovered PSD matrix to obtain natural frequencies and mode shapes. Notably, this centralized 3-stage forward-only approach minimizes processing and memory requirements at the node (local) level as well as wireless

FIGURE 1 | Flowchart of spectro-temporal compressive sensing framework (Klis and Chatzi, 2016b).

data communication payload within the WSN leading to low-complexity and low-energy consumption sensor nodes.

Elaborating on the mathematical details of PSBS approach, let $x(t)$ be a continuous in time t real-valued wide-sense-stationary random signal (or stochastic process) represented by the PSD function $P_x(\omega)$ band-limited to $2\pi/T$ in the frequency

domain ω. The multi-coset sampling strategy is adopted (e.g., Venkataramani and Bresler, 2001) in stage I of the approach to sample $x(t)$ at a rate lower than the Nyquist sampling rate $1/T$ (in Hz) as follows. Firstly, the uniform grid of Nyquist samples $x(nT)$, $n = 0, 1, 2, \ldots$ is divided into consecutive non-overlapping blocks of $\overline{N}$ samples each. Then, from each such block, only $\overline{M}$ ($< \overline{N}$)

FIGURE 2 | Flowchart of multi-channel power spectrum blind sampling approach for frequency domain OMA (see also Gkoktsi and Giaralis, 2019).

samples are acquired whose position is specified by the sampling pattern sequence with elements in ascending order
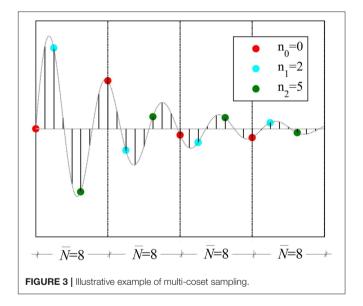
$$\mathbf{n} = [n_0 \ n_1 \ \cdots \ n_{\overline{M}-1}] \qquad (11)$$

taken as time independent. The resulting sampling is *periodic* with period N; *non-uniform* in time (excluding the special case in which $\mathbf{n}$ contains all possible even or odd numbers and $\overline{N}$ is even; *deterministic* since the position of the $\overline{M}$ *cosets* is defined *a priori* through the sequence $\mathbf{n}$ applied to all $\overline{N}$-length blocks; and *sub-Nyquist* with average sampling rate $\overline{M}/(\overline{N}T)$ (in Hz) (always below the Nyquist rate $1/T$ since $M < \overline{N}$). Notably, the multi-coset sampling rate is associated with the compression ratio (CR) $\overline{M}/\overline{N}$ ($0 \le \overline{M}/\overline{N} \le 1$), attaining lower values for higher signal compression levels. For illustration, **Figure 3** demonstrates multi-coset sampling with pattern $\mathbf{n} = [0, 2, 5]$ to a discrete-time signal partitioned into blocks of $N = 8$ length. This particular sampling acquires $\overline{M} = 3$ *cosets* of samples by taking the 1st (red), the 3rd (cyan), and the 6th (green) Nyquist sample from every block achieving CR of $\overline{M}/\overline{N} = 3/8 = 37.5\%$, that is, average sampling rate of 62.5% below Nyquist.

Mathematically, the samples of the m-th coset can be written as the output of the filtering operation

$$y^m[k] = \sum_{s=1-\overline{N}}^{0} g_m[s] \, x[k\overline{N}-s] \quad k=0,1,...,P-1 \quad (12)$$

where P is the total number of the $\overline{N}$-length blocks and the filter coefficients are given as

$$g_m[s] = \begin{cases} 1, & s = n_m \\ 0, & s \ne n_m \end{cases} \qquad (13)$$

FIGURE 3 | Illustrative example of multi-coset sampling.

in which $s = [1-N, 2-N, \ldots, 0]$ is arranged in descending order.

Consider, next, an array of D sensors and M cosets as shown in **Figure 2**. The cross-correlation sequences of response acceleration signals sampled at Nyquist rate, $x_i[\nu]$, from all $i = 1, 2, \ldots, D$ sensors are theoretically defined as

$$r_{x_i x_j}[\ell] = \mathrm{E}_x \left\{ x_i[\nu] \, x_j[\nu - \ell] \right\} \quad i,j = 1,2,...,D \, ; \ \ell \in \mathbb{Z} \quad (14)$$

where E is the mathematical expectation operator. It is herein assumed that the sequences in Equation (14) take on negligible

values outside the range $-L \leq \ell \leq L$. Further, the cross-correlation sequences of the compressed measurements $y_i^m[k]$ from all $m = 0, 1, \ldots, \overline{M} - 1$ cosets and $i = 1, 2, \ldots, D$ sensors, are written as

$$r_{y_i^a, y_j^b}[\ell] = \mathrm{E}\left\{ y_i^a[k] \, y_j^b[k - \ell] \right\}$$
$$i, j = 1, 2, ..., D \, ; \; a, b = 0, 1, ..., \overline{M} - 1 \, ; \; -L \leq \ell \leq L \quad (15)$$

It can be shown (Gkoktsi and Giaralis, 2019) that the sequences in Equations (14) and (15) are related by the following key equation

$$\mathbf{r}_{y_i y_j} = \mathbf{R}_g \mathbf{r}_{x_i x_j} \quad (16)$$

where $\mathbf{r}_{x_i x_j} \in \mathbb{R}^{\overline{N}(2L+1) \times D}$ is a matrix collecting all cross-correlation sequences of response acceleration signals $r_{x_i x_j}[\ell]$, $\mathbf{r}_{y_i y_j} \in \mathbb{R}^{\overline{M}^2(2L+1) \times D}$ is a matrix collecting all cross-correlation sequences of the compressed measurements $r_{y_i^a, y_j^b}[\ell]$, and $\mathbf{R}_g \in \mathbb{R}^{\overline{M}^2(2L+1) \times \overline{N}(2L+1)}$ is a sparse pattern correlation matrix populated by the multi-coset sampling pattern cross-correlations

$$r_{g_a, g_b}[\tau] = \sum_{s=1-\overline{N}}^{0} g_a[s] g_b[s - \tau] = \delta[\tau - (n_a - n_b)] \quad (17)$$

where $\delta[u] = 1$ for $u = 0$ and $\delta[u] = 0$ for $u \neq 0$. Note that Equation (16) defines an overdetermined system of linear equations which can be solved for $\mathbf{r}_{x_i x_j}$ without any sparsity assumptions, provided that $\mathbf{R}_c$ is full column rank. The latter is satisfied for $M^2 \geq N$ (Ariananda and Leus, 2012).

From the practical/computational viewpoint, the unbiased estimator

$$\hat{r}_{y_i^a, y_j^b}[\ell] = \frac{1}{P - |\ell|} \sum_{l=\max\{0,\ell\}}^{P-1+\min\{0,\ell\}} y_i^a[l] y_j^b[l - \ell] \quad (18)$$

can be readily employed to approximate the sequences in Equation (15) using all compressed measurements wirelessly transmitted to a central unit (server) from all D sensors as indicated in **Figure 2**. These estimates are collected in the matrix $\hat{r}_{y_i y_j} \in \mathbb{R}^{\overline{M}^2(2L+1) \times D}$. Next, an estimate of the response acceleration PSD matrix at discrete frequencies with frequency discretization step (resolution)

$$\Delta \omega = \frac{2\pi}{(2L+1)\overline{N}} \quad (19)$$

is computed at the server through the formula (Gkoktsi et al., 2015; Gkoktsi and Giaralis, 2019)

$$\hat{\mathbf{G}}_{x_i x_j} = \mathbf{F}_{(2L+1)\overline{N}} \left(\mathbf{R}_g^\mathrm{T} \overline{\mathbf{W}}^{-1} \mathbf{R}_g \right)^{-1} \mathbf{R}_g^\mathrm{T} \overline{\mathbf{W}}^{-1} \hat{\mathbf{r}}_{y_i y_j}, \quad (20)$$

where $\mathbf{F}_{(2L+1)\overline{N}} \in \mathbb{C}^{\overline{N}(2L+1) \times \overline{N}(2L+1)}$ is the standard DFT matrix. In the last equation, $\overline{\mathbf{W}}$ is a weighting matrix, and the superscript "−1" denotes matrix inversion. Ultimately, in stage III, the PSD matrix in Equation is treated by the standard FDD algorithm to estimate R structural mode shapes, $\hat{\phi}_r$, and natural frequencies, $f_r, r = 1, 2, \ldots, R$.

The critical parameters of the herein briefly reviewed PSBS approach regulating CR are the number of cosets, $\overline{M}$, and the length $\overline{N}$ of the blocks in **Figure 3**, subject to the two constraints $\overline{M} < \overline{N}$ and $\overline{M}^2 \geq \overline{N}$. Once the values of $\overline{M}$ and $\overline{N}$ are fixed, the weighting matrix $\overline{\mathbf{W}}$ in Equation and the sampling pattern $\mathbf{n}$ is determined by solving a constrained least-squares optimization problem as detailed in Tausiesakul and González-Prelcic (2013) relying on the criterion $\hat{\mathbf{r}}_{x_i x_j} = \arg \min_{\mathbf{r}_{x_i x_j}} || \hat{\mathbf{r}}_{y_i y_j} - \mathbf{R}_g \mathbf{r}_{x_i x_j} ||_{\overline{\mathbf{W}}}^2$, where $||\mathbf{a}||_{\overline{\mathbf{W}}}^2 = \mathbf{a}^\mathrm{T} \overline{\mathbf{W}} \mathbf{a}$ is the weighted version of the Euclidean norm.

ASSESSMENT FOR SIGNAL RECOVERY IN TIME AND IN FREQUENCY DOMAIN

The effectiveness and applicability of both considered approaches for vibration-based modal identification relies on the accuracy of their respective information recovery operations from compressed measurements. That is, time-domain signal reconstruction/recovery in the *STCS-rwPBDN* approach, and frequency domain PSD estimation/recovery in the PSBS-based approach. In this section, the performance of the above recovery operations is numerically assessed using field-recorded response acceleration data from an operational Wind Turbine (WT) in Lübbenau, Germany (Klis and Chatzi, 2016a). The considered structure was instrumented with wired high-accuracy MEMs accelerometer sensors located at the cross-section of the WT tower at 80 and 100 m height. The instrumentation layout of the WT is shown in **Figure 4**. Acceleration data were conventionally acquired at a uniform-in-time sampling rate of 200 Hz measured for ∼10 min every half an hour over a period of 29 days. For the purposes of this work, a small, arbitrarily chosen, sub-set of the recorded acceleration signals is compressed at different compression levels and processed via STCS-rwPBDN and PSBS approaches. PSD estimates and reconstructed signals in time domain are recovered from the compressed data by application of STCS-rwPBDN and PSBS approaches, respectively, while time-histories and non-compressed PSDs of the as-recorded data serve as a basis of comparison. It is expected that the assessment of PSBS information recovery in frequency domain will be most critical given that the level of signal stationarity of the considered data-set is relatively low while PSBS approach relies, theoretically, on signal stationary assumption.

The numerical assessment of both methods is performed using an acceleration time-series recorded on the 29/12/2013 (at 15:44 p.m.) along the North direction (i.e., y-axis in **Figure 4**) from the middle sensor in **Figure 4** located at 80 m height. The considered acceleration recording was uniformly acquired in time and it consists of $N = 172,420$ samples. Firstly, baseline adjustment is applied to the raw time-series to remove the mean value and other spurious low-frequency trends. Then, the time-series is band-limited within the frequency range of [0.10, 25.00 Hz] through filtering using a fourth-order Butterworth band-pass filter.
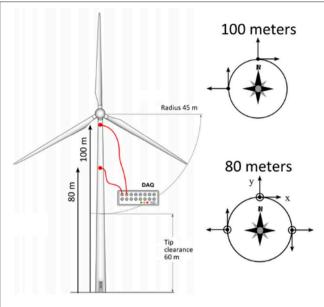
FIGURE 4 | Wind turbine tower and sensor instrumentation set-up (Chatzia and Spiridonakos, 2015).

STCS-rwBPDN Approach for Time Domain Signal Recovery

The time-domain reconstruction performance of the *STCS-rwBPDN* approach is assessed for two compression ratios at $CR = \{30, 45\%\}$. For a given WT acceleration response, the underlying signal support **U** is first computed to define the signal's sparsity level, K (i.e., number of components in the spectral domain), as well as the variance of the noisy component, i.e., the complementary set of the support (remaining part of the spectral representation). As elaborated upon in the work of Klis and Chatzi (2016a,b), this is used to prescribe error bounds on the reconstructed signal. For the two considered *CRs*, the obtained signal reconstruction estimates are illustrated in **Figure 5** for an acceleration time-window of 400 samples. Comparing the two panels **Figure 5**, it becomes evident that the increase in the number of transmitted samples results in narrowing the estimated maximal error bounds. **Figure 5** also demonstrates the potential of the *STCS-rwBPDN* approach, when applied in windows of non-stationary response signals, albeit necessitating higher compression rates than the conventional stationary case. The delivered error bounds allow for attributing some level of confidence on the undertaken signal reconstruction operation, which offers a benefit over the alternative (plain) *BPDN* approach adopted by O'Connor et al. (2014).

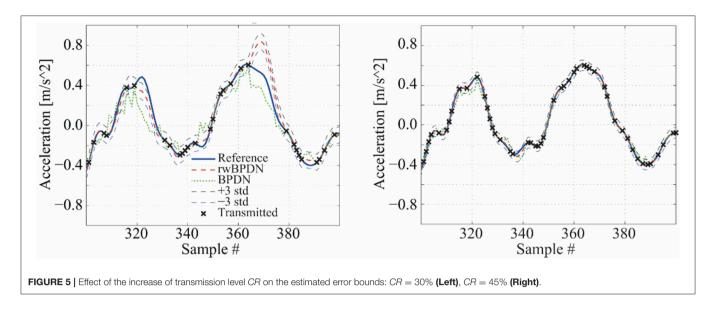## PSBS Approach for Frequency Domain PSD Signal Recovery

The efficacy of the PSBS approach is numerically evaluated herein in terms of recovering quality PSD estimates from computer-simulated compressed acceleration data. These compressed data are derived through the application of the multi-coset sampling pattern [section The Multi-Channel Power Spectrum Blind

Sampling (PSBS) Approach] to the corrected (i.e., baseline-adjusted and band-pass filtered), full-length ($N = 172,420$ samples) acceleration time-series shown in **Figure 6A**. The Welch periodogram (i.e., conventional PSD estimator) of the full-length time-series before and after band-pass filtering is further plotted in **Figure 6B**. The two PSDs are normalized to their peak value to facilitate a comparison and have been computed using 4,096 ($=2^{12}$) points in frequency domain, 8 overlapping segments with 50% overlap, and windowing with a Hanning envelop function. It is observed that peak PSD amplitude occurs at $\sim$1.4 Hz which is the dominant resonant frequency of the monitored WT. Further, it is seen that most important signal information lies in frequencies below 5 Hz, as PSD values above 5 Hz are negligible.

Given that the PSBS approach anticipates signal stationarity, it is deemed essential to undertake data qualification test to appraise the stationarity level of the recorded time-series considered. To this end, the corrected data **Figure 6A** is divided in seven time-frames of 2 min duration and the standard non-parametric reverse arrangement method (RAM) is used to test statistically the stationarity hypothesis (Bendat and Piersol, 2010). The outcome of RAM application to a representative 2 min long segment of the considered time-series is presented in **Figure 6C** demonstrating that the stationarity hypothesis is confirmed within a 95% confidence interval. Positive stationarity hypothesis is confirmed at similar confidence level for the rest of the 2 min-long segments of the data in **Figure 6A**. Therefore, this WT recorded data can be treated as wide-sense stationary at a high confidence level rendering the application of PSBS meaningful and appropriate.

Next, the WT time-series in **Figure 6A** is multi-coset sampled at three different CRs, 11, 21, and 31%, using the settings listed in **Table 1** and PSBS is applied to the compressed/sub-Nyquist multi-coset samples to obtain single-channel PSD function estimates using the PSD recovery formula in Equation. Specifically, for the case of $CR = 31\%$, the full-length acceleration data-series ($N = 172,420$ samples) is divided into $P = 10,776$ ($= N/\overline{N}$) blocks of length $\overline{N} = 16$ each, and from each block $\overline{M} = 5$ samples are selected according to the sampling pattern $\mathbf{n} = [0, 1, 2, 5, 8]$. These selected samples are collected in the compressed measurement sequences $y^m[k]$ ($m = 0, 1, 2, 3, 4; k = 1, 2, \ldots, P$) in Equation resulting in the acquisition and transmission of $M = 53,880$ compressed samples (i.e., 69% fewer samples compared to the original signal). The estimator $\hat{r}_{y_i^a, y_j^b}[\ell]$ in Equation is then computed for $i = j = 1$ (i.e., single-sensor trivial case) and $\ell \in [-40, 40]$ assuming support correlation parameter $L = 40$. The latter consideration enables PSD function recovery $\hat{G}_{xx} \in \mathbb{C}^{1296 \times 1}$ in Equation with frequency discretization step (resolution) $\Delta\omega = 4.85 \cdot 10^{-3}$ rad/s in Equation. Similar computational steps are taken for the cases of CR = 21 and 11%, based on the relevant parameters in **Table 1** which involve the acquisition of 79% (i.e., $M = 35,368$) and 89% (i.e., $M = 18,858$) fewer samples compared to the uniformly-sampled full-length signal, respectively.

Figure 7 plots PSD functions recovered from CR = {11, 31%} (solid red curves) in logarithmic and in linear scale. These
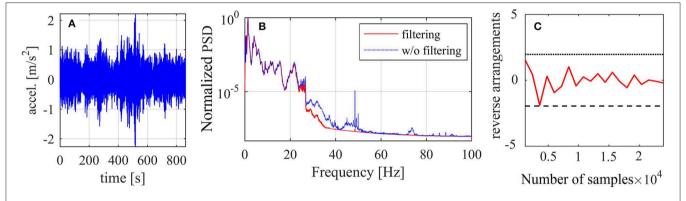
FIGURE 5 | Effect of the increase of transmission level *CR* on the estimated error bounds: *CR* = 30% **(Left)**, *CR* = 45% **(Right)**.

FIGURE 6 | (A) Base-line adjusted and filtered WT response acceleration data-series; **(B)** normalized Welch periodogram of raw and filtered WT response acceleration data-series in log (db-like) scale; **(C)** representative reverse arrangement output results for a 2-min long filtered data-series segment.

TABLE 1 | Adopted multi-coset sampling and PSBS settings.

Compression ratio (CR)	11%	21%	31%
Number of cosets ($\overline{M}$)	14	8	5
Length of data blocks ($\overline{N}$)	128	39	16
Sampling pattern sequence (**n**)	[0, 1, 2, 6, 8, 20, 29, 39, 47, 50, 53, 60, 63, 64]	[0, 1, 3, 7, 9, 14, 18, 19]	[0, 1, 2, 5, 8]
Correlation function support ($\overline{N}$ (2L+1))	1,152	1,287	1,296
PSD discretization step ($\Delta\omega$) in [rad/s]	5.45×10^{-3}	4.88×10^{-3}	4.85×10^{-3}

functions are normalized to their peak attained value to facilitate comparison against the standard Welch periodogram of the filtered full-length recorded time-series superposed on **Figure 7** (dotted blue curves) and normalized in the same manner. It is qualitatively observed that the PSBS-based recovered PSDs lie close to the PSD of the WT data for frequencies up to

5 Hz which take on non-negligible values, and therefore, contain dependable information for modal identification purposes under ambient/operational excitation, for the low CR value (high data compression level). Better quality point-wise matching between the PSBS-based PSDs and the "exact" (non-compressed) PSD of the WT data is achieved even beyond the 0–5 Hz frequency range for the highest CR value considered (i.e., lower data compression level) as expected.

To discuss further the level of accuracy of the proposed PSBS approach for modal properties identification **Table 2** reports the location of the three largest PSD ordinates obtained by simple peak-picking from the recovered functions via PSBS, $\hat{f}_{r,PSBS}$, as well as from the standard Welch periodogram applied to the non-compressed WT acceleration data (CR = 100%), $f_{r,Welch}$. Further, the percentage difference error

$$\frac{df_r}{f_r} = \frac{\left|\hat{f}_{r,PSBS} - f_{r,Welch}\right|}{f_{r,Welch}} \quad ; \quad r = 1, 2, 3, 4 \quad (21)$$

FIGURE 7 | Recovered PSDs using the PSBS approach for different CRs normalized to the peak values: **(A)** and **(B)** logarithmic (db-style) scale; **(C,D)** linear scale.
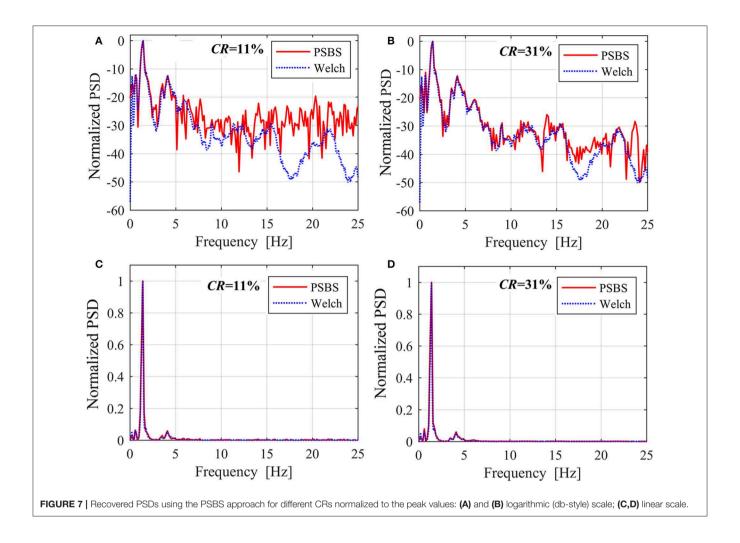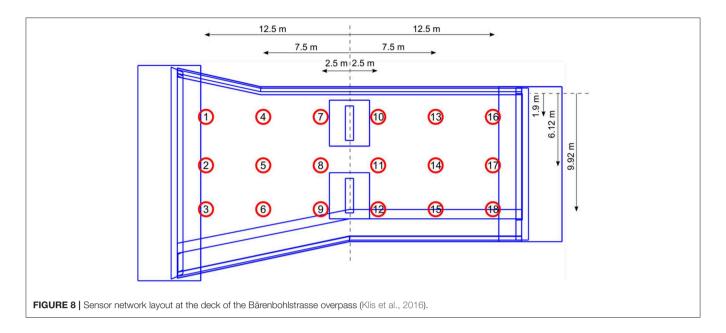
TABLE 2 | Frequency locations of peak PSD ordinates through peak-picking and percentage difference errors for the PSBS approach at various CRs and for Welch periodogram applied on the full-length signal (non-compressed) data-series.

CR	100% (Non-compressive/exact)	31%	21%	11%
f_1 [Hz]	0.635	0.635	0.624	0.570
(df_1/f_1)	–	(0.0%)	(1.7%)	(10.2%)
f_2 [Hz]	1.416	1.429	1.404	1.425
$(df_2/f_2$ [%])	–	(0.9%)	(0.8%)	(0.6%)
$f3$ [Hz]	4.102	4.127	4.056	4.131
$(df_3/f_3$ [%])	–	(0.6%)	(1.1%)	(0.7%)

is also reported as a measure of the quality of the recovered PSDs via the PSBS method. It is seen that the location of the two most prominent PSD peaks ($r = 2, 3$) is retrieved with <1% error by the PSBS approach for signal compression level as low as 89% below the sampling rate of the original data series. However, the accuracy drops as CR reduces (compression level increases) for the least prominent peak, $r = 1$, corresponding to an inadequately excited vibration mode whose detection is inherently a challenging task.

ASSESSMENT FOR MODE SHAPE EXTRACTION UNDER OPERATIONAL LOADING CONDITIONS

In this section, the effectiveness of STCS-rwPBDN and PSBS approaches for extracting modes of vibration and natural frequencies is numerically assessed within the OMA context. To this aim, response acceleration time-histories field recorded in a typical highway overpass open to traffic are used. The considered bridge is the Bärenbohlstrasse overpass in Zürich, Switzerland. The structure is 30.90 m long and fairly symmetric along its longitudinal direction. It consists of a solid prestressed-slab with two equal-length spans of 14.75 m each. The deck is supported in all directions at mid-span and in one of the two abutments, while it is only supported in the vertical and transverse directions at the second abutment. The deck was instrumented with a network of 18 conventional wired accelerometers recording vertical acceleration time-histories at 200 Hz sampling rate for ~10 min per hour from 12th July 2013 to 26th July 2014. The layout of the sensor network deployment is shown in **Figure 8**; more details about the bridge and the monitoring campaign can be found in Klis et al. (2016).

FIGURE 8 | Sensor network layout at the deck of the Bärenbohlstrasse overpass (Klis et al., 2016).

Herein, the first 2 min-long recordings of a dataset of 18 vertical acceleration time-series simultaneously recorded on 19/06/2014 between 15:08:54 and 15:17:51 from each of the 18 sensors of the network are used. The dataset is pre-processed in the same way as the WT data-series case-study in section STCS-rwBPDN Approach for Time Domain Signal Recovery. That is, they are baseline adjusted and band-limited within [0.15, 50 Hz] frequency range using a band-pass 4th-order Butterworth filter. For illustration, **Figure 9** plots the band-pass filtered acceleration response signal recorded at sensor #13, together with its magnitude Fourier spectrum. Further, representative results from RAM application to a 1 min long segment of this record is provided demonstrating a very high level of data stationarity (i.e., much higher than the WT data-set; see **Figure 6C** for comparison).

Next, the first 2 min of the 18 time-series are downsampled at 100 Hz and treated by the STCS-rwPBDN and PSBS approaches. Starting from the STCS-rwPBDN approach, the considered dataset is first partitioned into $R = 29$ windows (frames) of $N_R =$ 400 samples, and each window is projected into the spectral (Fourier) domain as indicatively shown in **Figure 10A** for an arbitrarily chosen data-frame of sensor #1 time-series. Following the STCS-rwPBDN methodology in section Spectro-Temporal Compressive Sensing (STCS) Approach via *rwBPDN*, the spectral (Fourier) coefficients per data frame are then thresholded with a value $\epsilon_{ij} = \epsilon_l \|\mathbf{c}_{ij}\|_1 / N_R$, $j = 1 \ldots R$, which pertains to $\epsilon_l = 1.5$, yielding the spectral domain elements illustrated in **Figure 10A**. The selected support elements are further used to form a weighting matrix W_{ij} per data frame. Considering next two different CRs at {36%,11%}, the compressed samples y_i (denoted with a cross in **Figure 10B**) are selected and used to retrieve the reconstructed time-domain sequence plotted in **Figure 10B** by a broken line. The standard Natural eXcitation Technique (NeXT) combined with the Eigensystem Realization Algorithm (ERA) are then used to extract estimates of the bridge deck mode shapes,

$\hat{\phi}_r$ $(r = 1, 2, \ldots)$, and natural frequencies, $\hat{f}_r$ $(r = 1, 2, \ldots)$, within an OMA context (Brincker and Ventura, 2015).

Moreover, the same dataset is treated by the PSBS approach using the same procedure and settings as in the WT case-study in **Table 1** to recover the PSD matrices $\hat{G}_{x_i x_j} \in \mathbb{C}^{\overline{N}(2L+1) \times 18}$ in Equation for CR = {31, 21, 11%}. The standard FDD algorithm of OMA (Brincker and Ventura, 2015) is applied to these matrices to find estimates of estimates of mode shapes, $\hat{\phi}_r (r = 1, 2, \ldots)$, and natural frequencies, $\hat{f}_r$ $(r = 1, 2, \ldots)$, of the monitored bridge. Indicatively, the first row of panels of **Figure 11** plots the first four estimated mode shapes of the bridge for CR = 11% using the PSBS with FDD approach.

The quality/accuracy of modal properties extracted through the STCS-rwPBDN and PSBS approaches is assessed by comparison to natural frequencies, f_r $(r = 1, 2, \ldots)$, and mode shapes, ϕ_r $(r = 1, 2, \ldots)$, obtained by application of the standard FDD to the full-length (non-compressive) dataset of recorded acceleration time-histories which are treated as the "exact" ones. The second row of panels of **Figure 11** plots the first four exact mode shapes and further reports the corresponding natural frequencies. **Table 3** reports percentage difference errors of the first four natural frequencies of the bridge deck obtained through coupling the STCS-rwPBDN with NeXT-ERA as well as the PSBS with FDD for different CRs with respect to the exact (non-compressive) ones as per Equation (21). It further collects the corresponding Modal Assurance Criterion (*MAC*) values defined by (Brincker and Ventura, 2015)

$$MAC = \frac{\left| \phi_r^T \hat{\phi}_r \right|^2}{\|\phi_r\|_2^2 \left\| \hat{\phi}_r \right\|_2^2} \quad r = 1, 2, 3, 4 \qquad (22)$$

to quantitatively compare the mode shapes extracted through the two compressive/sub-Nyquist approaches considered for different CRs with the exact mode shapes. As a commonly used
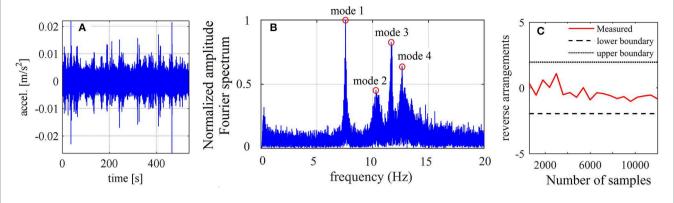
FIGURE 9 | (A) Base-line adjusted and filtered bridge acceleration data-series from sensor #13 in **Figure 8**; **(B)** normalized Fourier amplitude spectrum of the data-series in **(A)**; **(C)** representative reverse arrangement output results for a 2-min long filtered data-series segment.
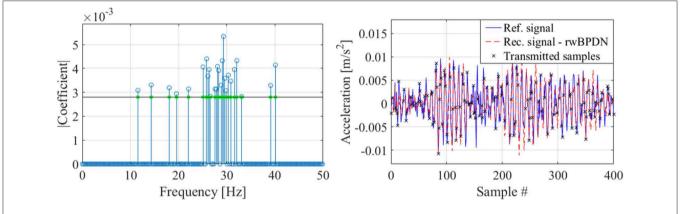

FIGURE 10 | Spectral domain projection **(left)** and time-domain recovery **(right)** of data-frame #4, channel #1 at CR = 36%. Crosses indicate transmitted samples used in the recovery process.

criterion, estimated mode shapes with $MAC > 0.90$ are regarded to be acceptably close to the exact ones.

By examining the numerical data in **Table 3**, it is seen that both STCS-rwPBDN and PSBS approaches are quite accurate in identifying natural frequencies as the error df/f is well below 1% even for the lowest CR = 11% value corresponding to average sampling rate of 89% below the Nyquist rate which equals to 100 Hz for the dataset considered. Further, the PSBS approach yields accurate mode shapes across the board for CR as low as 21%. For the lowest CR (=11%), PSBS is still capable of extracting the 1st and 3rd modes with acceptable accuracy, as can be visually appreciated by comparing the mode shapes in **Figures 11A,C** with **Figures 11E,G**, respectively. However, PSBS fails to pass the $MAC > 0.90$ criterion for 2nd and 4th modes for CR = 11% as highlighted in boldface font in **Table 3** (compare also **Figures 11B,D** with **Figures 11F,H**). This is readily attributed to the fact that 2nd and 4th modes are significantly less excited than 1st and 3rd modes as evidenced by the amplitude of the respective Fourier coefficients in **Figure 9B**. Higher than 11% CR (i.e., larger number of measurements) is required for the PSBS approach to accurately probe into the least excited 2nd and 4th modes. On the antipode, the STCS-rwPBDN

approach provides good estimates for all four modes even at CR = 11%.

To highlight the practical merit of considering reduced CR values, estimates of daily energy consumption and battery lifetime savings for a single wireless sensor node of the WSN in **Figure 8** are further reported in **Table 4**. The data account for only data transmission power requirement as this is by far the most energy demanding sensor operation (e.g., Lynch, 2007). The reported estimates are based on the assumption that each sensor acquires 2 min long acceleration signals at Nyquist rate (CR = 100%) with Fs = 100 Hz (Ts = 0.01 s) under operational conditions every 1 h (i.e., a dataset of $Q = 24$ signals are collected daily per sensor with each signal comprising 12,000 measurements for CR = 100%). Power consumption during transmission of P_t = 103.8 mW is taken based on the specification of a typical wireless sensor used for SHM: the WiseNode v4 developed by Novakovic et al. (2009). **Table 4** reports transmission time, energy consumption, and battery lifetime for three different CRs previously considered in **Table 3**. For illustration, computations pertaining to the case of CR = 11% are presented in detail for which only 12,000 × 0.11 = 1,320 compressed measurements per hour are wirelessly transmitted.

FIGURE 11 | Mode shapes of Bärenbohlstrasse overpass: **(A–D)**: estimated using the PSBS approach for CR = 11%; **(E–H)**: "exact" (non-compressive) by application of FDD to the full-length recorded data.
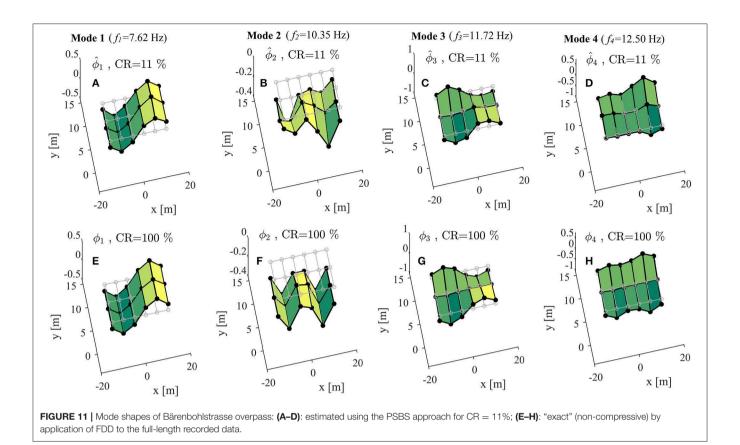
TABLE 3 | Quantitative assessment of the accuracy of natural frequencies and mode shapes for the bridge case-study obtained by the PSBS with FDD and by the STCS-rwPBDN with NeXT-ERA approaches for different CRs vis-à-vis standard non-compressive FDD approach.

	Non-compressive FDD	STCS-rwPBDN plus NeXT-ERA				PSBS plus FDD					
	CR = 100%	CR = 36%		CR = 11%		CR = 31%		CR = 21%		CR = 11%	
Mode	f [Hz]	df/f [%]	MAC	df/f [%]	MAC	df/f [%]	MAC	df/f [%]	MAC	df/f [%]	MAC
1	7.62	0.63	1.00	0.52	0.98	0.57	1.00	0.20	0.99	0.68	0.99
2	10.35	0.18	0.98	0.32	0.98	0.04	0.98	0.32	0.91	0.04	**0.89**
3	11.72	0.19	0.99	0.14	0.99	0.24	0.99	0.35	0.98	0.57	0.94
4	12.50	1.22	0.96	0.78	0.94	0.15	0.98	0.31	0.93	0.17	**0.64**

Assuming that ADC units with 16 bits (i.e., 2 bytes) resolution are used, I_{FWD} = 2,640 bytes of data package information are generated per compressed sequence taking $t = (I_{FWD}/I_{t1}) \times t_1$ = 7.54 s to be wirelessly transmitted to the server, where $I_{t1} = 7$ bytes is the information carried within one data package and $t_1 = 0.02$ s is the time required for package transmission (Novakovic et al., 2009). Thus, $t_{tot} = Q \times 7.54 = 181$ s (or 0.05 h) are required for the daily transmission of all compressed acceleration response data, consuming E_{tot}= $P_t \times t_{tot}$ = 18.79 J of energy per day. It is further assumed that sensor energy supply of 3 V comes from two AA-sized batteries with nominal voltage V_n = 1.5 V and capacity C_n = 3,000 mAh, providing energy E_b= 64,800 J. A continuous discharge current is taken to occur in the batteries resulting in ξ = 1% annual energy loss. Then, sensor battery lifetime, given by

$$T_b = \frac{E_b}{E_{tot} + E_b \times \xi/365},\qquad(23)$$

is estimated as T_b= 104.8 months.

Similar calculations are performed to estimate E_{tot} and T_b for CR = 21, 31% as well as CR = 100% (non-compressive transmission) shown in **Table 4**. The latter case is the one most widely considered in the literature in comparative studies on energy savings quantification in wireless sensors (e.g., O'Connor et al., 2013, 2014; Klis and Chatzi, 2016b). In this respect, **Table 4** reports energy reduction and battery gain ratio for all CR < 100%

TABLE 4 | Daily sensor energy consumption and battery lifetime gains due to wireless data transmission for various CRs.

Compression ratio (CR)	100% (non-compressive)	31%	21%	11%
Transmission time (t_{tot}) [h]	0.46	0.14	0.10	0.05
Energy spent (E_{tot}) [J]	170.83	52.96	35.87	18.79
Energy reduction (ER)	–	69%	79%	89%
Battery life (T_b) [months]	12.5	39.4	57.3	104.8
Battery gain Ratio (BR)	–	3.15	4.58	8.38

examined with respect to CR = 100% given as

$$ \mathrm{ER} = \frac{E_{tot}|_{CR=100} - E_{tot}|_{CR}}{E_{tot}|_{CR=100}} \times 100 \% \text{ and} $$

$$ \mathrm{T}_b = \frac{T_b|_{CR}}{T_b|_{CR=100}}, \qquad (24) $$

respectively. Evidently, battery life expectancy increases dramatically as CR reduces: it more than triples for CR = 31% compared to non-compressive sampling/transmission, while it increases more than 8 times for CR = 11%. In this respect, through collective consideration of the data in **Tables 3**, **4**, it can be concluded that the considered approaches effectively support more sustainable wireless monitoring systems having reduced maintenance costs and environmental impact associated with sensors battery replacement which can be scheduled at much longer intervals without significant deterioration to the accuracy of the estimated modal properties compared to Nyquist data sampling.

Note, however, that in a practical setting, the choice of CR (and corresponding battery lifetime gains) is normally dictated by the sought level of accuracy in extracting modal properties according to the monitoring purpose and objectives. If accurate modal properties estimation in the absolute sense is desired (e.g., for updating computational models of as-built structures, or for designing/assessing the performance of vibration control devices, such as tuned mass dampers, to reduce dynamic response of structures) higher CR values should be adopted (e.g., CR > 31%). In such cases, battery lifetime gains may be relatively low but, at the same time, these gains may be a less important practical consideration. On the antipode, lower CR values (e.g., CR = 21% or lower) may be adopted in monitoring campaigns for which extending sensor battery lifetime becomes a priority over modal extraction accuracy. One such example is in long-term/permanent structural monitoring deployments aiming to detect structural damage (e.g., due to natural deterioration or after an extreme event), in which case reducing battery replacement frequency, and thus maintenance costs, becomes important and may be a main criterion for installing a monitoring system in the first place (e.g., O'Connor et al., 2014), while accuracy of modal properties in the absolute

sense is less important since changes to modal properties (as a function of environmental conditions) are of interest.

In every case, the data furnished in **Tables 3**, **4** are only indicative and should be used/interpreted comparatively rather than in an absolute. Indeed, recorded measurements considered to derive modal properties have been obtained by a wired sensor network and, therefore, do not account for the influence of errors that may be encountered in WSNs, such as loss of synchronization. Moreover, power consumption (and thus battery lifetime gains) varies from sensor to sensor in a WSN and is dependent on several factors including environmental conditions, distance from sensors to base station, data communication protocols, etc. In this regard, field deployment of WSNs operating on PSBS and STCS-rwPBDN is required to appraise the quality of modal properties and battery gains in an absolute application-specific sense; such consideration falls outside the scope of this work.

CONCLUDING REMARKS

The applicability and performance of two recently proposed approaches for output-only modal identification supporting low energy consumption wireless sensors has been comparatively demonstrated through numerical assessment using field recorded acceleration data. Both the approaches aim to reduce wireless data transmission payloads by considering compressed structural acceleration responses acquired non-uniformly in time at sub-Nyquist average sampling rates. The first, STCS-rwBPDN, approach aims to recover acceleration time-histories in time-domain from low-rate randomly acquired measurements using the rwBPDN algorithm of compressing sensing. The accuracy and efficiency of this operation requires knowledge of the signal support in the frequency domain prior to transmission of compressed measurements from sensor nodes to a central server where time-domain reconstruction takes place. This knowledge is gained through sampling and interrogation of full-length acceleration data at the sensing nodes as well as sensors/server exchange of pertinent information. In this regard, STCS-rwBPDN can recover the time trace of response acceleration signals in a deterministic setting and, therefore, can be coupled at the post-processing back-end with any standard OMA technique for modal properties extraction. Nevertheless, this flexibility comes at the cost of a relatively sophisticated wireless data communication strategy as well the necessity to sample signals at Nyquist frequency or above at sensors front-end. The second, PSBS, approach is effectively a spectral estimation technique aiming to recover second-order statistics (i.e., correlation or PSD functions) of response acceleration signals treated as stationary random processes and acquired through low-rate deterministic non-uniform-in-time multi-coset sampling. Compared to STCS-rwBPDN, the main practical advantage of the PSBS-based approach is its simplicity of wireless communication within WSNs as well as minimal on-sensor data interrogation. Low-rate multi-coset samples can be acquired using some pre-specified sampling pattern at each sensor and communicated as-recorded directly to a server. This high level of data transmission simplicity

is made possible by the inherent signal agnostic attribute of PSBS which does not require any prior knowledge about signal spectral support. However, PSBS approach cannot retrieve time traces of the acquired signals and this limits the system identification methodologies that can be applied at the back end of the approach to those relying on only second-order signal statistics for modal properties extraction. One such method is the FDD which was herein coupled with PSBS to deliver mode shapes and natural frequencies directly from the low-rate multi-coset sampled response accelerations.

The validation of the two approaches was carried out by considering field-recorded acceleration data obtained from conventional wired sensor deployments in an operating on-shore wind turbine and in a highway overpass (bridge) open to traffic. The recorded data have been compressed to different levels (CRs) and processed by both approaches. PSBS captured successfully salient frequency domain information for the dataset of the wind turbine for CR as low as 11% (i.e., using 89% less measurements from the conventionally sampled dataset). This demonstrates the potential of the method to treat real-life data that may deviate from perfect stationary signal conditions. Similarly, STCS-rwBPDN was shown to recover faithfully time traces of the wind turbine data set at same low CR levels (11%). In view of these results, it is concluded that both methods are equally promising for SHM of wind turbines using low-rate acceleration measurements. Moreover, STCS-rwBPDN coupled with standard NeXT-ERA was able to retrieve quality estimates of mode shapes and natural frequencies of the bridge case-study again at CR = 11%. PSBS was also able to capture with high accuracy the same mode shapes for CR = 21% while only the two most significant ones were retrieved at CR = 11% satisfactorily.

In view of the herein reported numerical results, it is concluded that both the considered approaches are capable for accurate output-only system identification of large-scale civil infrastructure while being, to a good extend, complementary. Moreover, it is noted that both approaches can be used to acquire alternative types of signals to acceleration data, such as tilt measurements and dynamic strains considered in SHM. It is thus envisioned that smart sensing nodes may incorporate both these approaches for reducing data transmission payloads in WSNs which will allow operators to switch between the two depending on their monitoring needs at any given time: time-series recovery at, perhaps, some increased data transmission requirements and more intense on-sensor processing or modal properties recovery at minimum wireless data exchange and with minimum on-sensor data interrogation.

Still, note that all datasets considered in this work pertain to wired sensors and, therefore, are free from errors that are more common in WSNs, such as missing data or gaps in data due to data loss in wireless transmission, loss of synchronization among sensors, etc. The extent of such errors and its potential impact to the quality of monitoring (e.g., accuracy of extracted mode shapes and natural frequencies) is application-specific depending on factors, such as the technology and quality of the sensor nodes used, the topology of WSN, the nature and scale of the monitored structure, the environmental conditions etc. Moreover, the same factors influence sensor energy consumption and ultimately battery lifetime. In this regard, consideration of long-term real-life field deployments of WSNs operating on the examined approaches is further warranted to verify the accuracy and battery life prolongation of the approaches for full-fledged monitoring of large-scale civil engineering structures. This consideration is left for future work.

DATA AVAILABILITY

The datasets generated for this study are available on request to the corresponding author.

AUTHOR CONTRIBUTIONS

AG and EC conceived the study. KG performed all data processing related to the PSBS approach. RK and VD performed all data processing related to the STCS approach. KG produced a first draft of the article which was finalized by critical input by AG and EC on introduction, results interpretation, and concluding remarks.

FUNDING

ACKNOWLEDGMENTS

REFERENCES

Ariananda, D. D., and Leus, G. (2012). Compressive wideband power spectrum estimation. *IEEE Trans. Signal Proc.* 60, 4775–89. doi: 10.1109/TSP.2012.2201153

Avendaño-Valencia, L. D., Chatzi, E. N., Koo, K. Y., and Brownjohn, J. M. W. (2017). Gaussian process time-series models for structures under operational variability. *Front. Built Environ.* 3:69. doi: 10.3389/fbuil.2017.00069

Bao, Y., Beck, J. L., and Li, H. (2010). Compressive sampling for accelerometer signals in structural health monitoring. *Struct. Health Monitor.* 10, 235–246. doi: 10.1177/1475921710373287

Becker, S., Bobin, J., and Candès, E. J. (2011). NESTA: a fast and accurate first-order method for sparse recovery. *SIAM J. Imaging Sci.* 4, 1–39. doi: 10.1137/090756855

Bendat, J. S., and Piersol, A. G. (2010). *Random Data: Analysis and Measurement Procedures. 4th Edn.* Hoboken, NJ: John Wiley & Sons Inc.

Brincker, R., and Ventura, C. E. (2015). *Introduction to Operational Modal Analysis.* Hoboken, NJ: John Wiley & Sons Inc.

Candès, E. J., and Plan, Y. (2011). A probabilistic and RIPless theory of compressed sensing. *IEEE Trans. Inform. Theory* 57, 7235–7254. doi: 10.1109/TIT.2011.2161794

Candès, E. J., and Romberg, J. (2007). Sparsity and incoherence in compressive sampling. *Inv. Probl.* 23, 969–985. doi: 10.1088/0266-5611/23/3/008

Candès, E. J., Romberg, J., and Tao, T. (2006). Robust uncertainty principles: exact signal reconstruction from highly incomplete frequency information. *IEEE Trans. Inform. Theory* 52, 489–509. doi: 10.1109/TIT.2005.862083

Candès, E. J., and Tao, T. (2006). Near-optimal signal recovery from random projections; universal encoding strategies? *IEEE Trans. Inform. Theory* 52, 5406–5425. doi: 10.1109/TIT.2006.885507.

Chatzia, E. N., and Spiridonakos, M. D. (2015). "Structural identification and monitoring based on uncertain/limited information," in *EVACES'15, 6th International Conference on Experimental Vibration Analysis for Civil Engineering Structures* (Dübendorf). doi: 10.1051/matecconf/20152401003

Donoho, D. L. (2006). Compressed sensing. *IEEE Trans. Inform. Theory* 52, 1289–1306. doi: 10.1109/TIT.2006.871582

Eslani, N., Aghagolzadeh, A., and Andargoli, S. M. H. (2014). "Recovery of compressive video sensing via dictionary learning and forward prediction," in *7th International Symposium on Telecommunications* (Tehran). doi: 10.1109/ISTEL.2014.7000819

Farrar, C. R., and Worden, K. (2012). *Structural Health Monitoring: A Machine Learning Perspective.* Hoboken, NJ: John Wiley & Sons Inc.

Fuentes, R., Mineo, C., Pierce, S. G., Worden, K., and Cross, E. J. (2019). A probabilistic compressive sensing framework with applications to ultrasound signal processing. *Mech. Syst. Signal Process.* 117, 383–402. doi: 10.1016/j.ymssp.2018.07.036.

Gkoktsi, K. (2018). *Compressive techniques for sub-Nyquist data acquisition & processing in vibration-based structural health monitoring of engineering structures* (PhD Thesis). University of London, London.

Gkoktsi, K., and Giaralis, A. (2017). Assessment of sub-Nyquist deterministic and random data sampling techniques for operational modal analysis. *Struct. Health Monitor.* 16, 630–646. doi: 10.1177/1475921717725029

Gkoktsi, K., and Giaralis, A. (2019). A multi-sensor sub-Nyquist power spectrum blind sampling approach for low-power wireless sensors in operational modal analysis applications. *Mech. Syst. Signal Process.* 116, 879–899. doi: 10.1016/j.ymssp.2018.06.049

Gkoktsi, K., Giaralis, A., and TauSiesakul, B. (2016). "Sub-Nyquist signal-reconstruction-free operational modal analysis and damage detection in the presence of noise," in *Proceedings of SPIE on Sensors and Smart Structures Technologies for Civil, Mechanical, and Aerospace Systems,* 9803. doi: 10.1117/12.2219194

Gkoktsi, K., Tausiesakul, B., and Giaralis, A. (2015). "Multi-channel sub-Nyquist cross-spectral estimation for modal analysis of vibrating structures," in *Proceedings of the 22nd International Conference on Systems, Signals and Image Processing,* 287–290.

Klis, R., and Chatzi, E. N. (2016a). Data recovery via hybrid sensor networks for vibration monitoring of civil structures. *Int. J. Sust. Mater. Struct. Syst.* 2, 161–184. doi: 10.1504/IJSMSS.2015.078373

Klis, R., and Chatzi, E. N. (2016b). Vibration monitoring via spectro-temporal compressive sensing for wireless sensor networks. *Struct. Infrastr. Eng.* 13, 195–209. doi: 10.1080/15732479.2016.1198395

Klis, R., Chatzi, E. N., and Spiridonakos, M. (2016). "Validation of vibration monitoring via spectro-temporal compressive sensing for wireless sensors networks using bridge deployment data," in *Proceedings of the 8th International Conference on Bridge Maintenance, Safety and Management (IABMAS 2016).*

Limongelli, M. P., Chatzi, E. N., Döhler, M., Lombaert, G., and Reynders, E. (2016). Towards extraction of vibration-based damage indicators," in *EWSHM-8th European Workshop on Structural Health Monitoring* (Bilbao).

Lynch, J. P. (2007). An overview of wireless structural health monitoring for civil structures. *Philosoph. Trans. R. Soc.* A365, 345–372. doi: 10.1098/rsta.2006.1932

Nagayama, T., Spencer B. F. Jr., and Jennifer, A., Rice. (2009). Autonomous decentralized structural health monitoring using smart sensors. *Struct. Control Health Monitor.* 16, 842–859. doi: 10.1002/stc.352

Nesterov, Y. (2005). Smooth minimization of non-smooth functions. *Math. Programm.* 103, 127–152. doi: 10.1007/s10107-004-0552-5

Novakovic, A., Meyer, J., Bischoff, R., Feltrin, G., Motavalli, M., El-Hoiydi, A., et al. (2009). *Low Power Wireless Sensor Network for Monitoring Civil Infrastructure.* Technical Report, Empa, Swiss Federal Laboratories for Materials Testing and Research. CSEM, Swiss Center for Electronics and Microtechnology.

O'Connor, S. M., Lynch, J. P., and Gilbert, A. C. (2013). *Implementation of a Compressive Sampling Scheme for Wireless Sensors to Achieve Energy Efficiency in a Structural Health Monitoring System,"* in *SPIE Smart Structures and Materials + Nondestructive Evaluation and Health Monitoring* SPIE, 11.

O'Connor, S. M., Lynch, J. P., and Gilbert, A. C. (2014). Compressed sensing embedded in an operational wireless sensor network to achieve energy efficiency in long-term monitoring applications. *Smart Mater. Struct.* 23:085014. doi: 10.1088/0964-1726/23/8/085014

Park, J. Y., Wakin, M. B., and Gilbert, A. C. (2014). Modal analysis with compressive measurements. *IEEE Trans. Signal Process.* 62, 1655–1670. doi: 10.1109/TSP.2014.2302736

Razaviyayn, M., Tseng, H.-W., and Luo, Z.-Q. (2014). "Dictionary learning for sparse representation: complexity and algorithms," *Proceedings-ICASSP, IEEE International Conference on Acoustics, Speech and Signal Processing* (Florence). doi: 10.1109/ICASSP.2014.6854604

Reynders, E., Gersom, W., and De Roeck, G. (2013). Output-only structural health monitoring in changing environmental conditions by means of nonlinear system identification. *Struct. Health Monitor.* 13, 82–93. doi: 10.1177/1475921713502836

Shi, H., Worden, K., and Cross E. J. (2016). A non-linear cointegration approach with applications to structural health monitoring. *J. Phys.* 744:012025. doi: 10.1088/1742-6596/744/1/012025

Straub, D., Eleni, C., Elizabeth, B., Wim, C., Döhler, M., Faber, M. H., et al. (2017). "Value of information: a roadmap to quantifying the benefit of structural health monitoring," in *ICOSSAR-12th International Conference on Structural Safety & Reliability* (Vienna).

Tausiesakul, B., and González-Prelcic, N. (2013). "Power spectrum blind sampling using minimum mean square error and weighted least squares," in *2013 Asilomar Conference on Signals, Systems and Computers* (Pacific Grove, CA), 153–157.

Vaswani, N., and Zhan, J. (2016). Recursive recovery of sparse signal sequences from compressive measurements: a review. *IEEE Trans. Signal Proc.* 64, 3523–3549. doi: 10.1109/TSP.2016.2539138

Venkataramani, R., and Bresler, Y. (2001). Optimal sub-Nyquist nonuniform sampling and reconstruction for multiband signals. *IEEE Trans. Signal Process.* 49, 2301–2313. doi: 10.1109/78.950786

Wang, W., Wang, P., Zhou, W., and Li, H. (2015). "The study of damage identification based on compressive sampling," in *Proceedings SPIE 9437, Structural Health Monitoring and Inspection of Advanced Materials, Aerospace, and Civil Infrastructure 2015, 94371L.* doi: 10.1117/12.2084061

Wang, Y., and Hong, H. (2015). Damage identification scheme based on compressive sensing. *J. Comp. Civil Eng.* 29:04014037. doi: 10.1061/(ASCE)CP.1943-5487.0000324

Yang, Y., and Nagarajaiah, S. (2015). Output-only modal identification by compressed sensing: non-uniform low-rate random sampling. *Mech. Syst. Signal Process.* 56–57, 15–34. doi: 10.1016/j.ymssp.2014.10.015

Zou, Z., Bao, Y., Li, H., and Spencer, B. F. (2015). Embedding compressive sensing-based data loss recovery algorithm into wireless smart sensors for structural health monitoring. *IEEE Sens. J.* 15, 797–808. doi: 10.1109/JSEN.2014.2353032